KSME

Springer

Journal of Mechanical Science and Technology 36 (2) 2022

Original Article
DOI 10.1007/s12206-022-0142-6

Keywords:
· Autonomous mobile robot
· Contact angle estimation
· Kinematic analysis
· Slip control

Correspondence to:
Hyungpil Moon
hyungpil@skku.edu

Citation:
Pico, N., Jung, H., Medrano, J., Abayebas, M., Kim, D. Y., Hwang, J.-H., Moon, H. (2022). Climbing control of autonomous mobile robot with estimation of wheel slip and wheel-ground contact angle. Journal of Mechanical Science and Technology 36 (2) (2022) 959~968.
http://doi.org/10.1007/s12206-022-0142-6

Received May 21st, 2021
Revised September 10th, 2021
Accepted October 13th, 2021

† Recommended by Editor
Ja Choon Koo

Climbing control of autonomous mobile robot with estimation of wheel slip and wheel-ground contact angle

Nabih Pico[1,2], Hong-ryul Jung[1], Juan Medrano[1], Meseret Abayebas[1,3], Dong Yeop Kim[4], Jung-Hoon Hwang[4] and Hyungpil Moon[1]

[1]Department of Mechanical Engineering, Sungkyunkwan University, 2066, Seobu-ro, Jangan-gu, Suwon-si, Gyeonggi-do, Korea, [2]Facultad de Ingeniería en Electricidad y Computación, Escuela Superior Politécnica del Litoral, ESPOL, Campus Gustavo Galindo, Guayaquil 09-01-5863, Ecuador, [3]School of Electrical and Computer Engineering, Addis Ababa Institute of Technology, Addis Ababa University, P.O. Box 385, Addis Ababa, Ethiopia, [4]Intelligent Robotics Research Center, Korea Electronics Technology Institute (KETI), 655, Pyeongcheon-ro, Bucheon-si, Gyeonggi-do, Korea

Abstract The objective of this work is to control a delivery robot equipped with a passive bogie that can successfully climb up steps of various sizes and move on uneven terrain in outdoor environments. The kinematic model of a six-wheel mobile robot is described in detail. Jacobian matrices and inverse kinematics are obtained to get the velocity of each wheel based on the desired velocity of the robot center of mass in conjunction with the terrain information obtained by the onboard sensors according to the contact angle estimation between the wheel and ground. A slip control is implemented based on slip ratio to adjust the wheel velocity when the slip is detected. Simulation and experimental results verify the effectiveness of the approach that enables the robot autonomously climbing up on different steps and uneven terrain.

1. Introduction

Autonomous mobile robots are a rapidly developing field in robotics known for solving many of today's problems. Their development is facilitated by their capability to operate in unknown environments and navigate without human intervention or slight intervention [1-4]. Sensor and control algorithms allow the robot to multitask and perform in applications like space missions, where the motion and performance based on kinematic models are analyzed [5-7]. Transportation of objects is another important task for mobile robots. Certain solutions are required to create cooperative robots that can handle and transport payloads [8-10]. Furthermore, search and rescue applications require mobile robots to perceive and operate in difficult environments such as collapsed buildings [11-14]. Extant research has focused on overcoming obstacles, maintaining their stability, adapting to different terrains [15-18], and safe and secure navigation, like in a complex crowded environment predicting the future actions of humans by developing danger zones [19]. The most common mechanisms used in wheeled robots include rocker-bogie, RCL-E, and CRAB [20, 21]. The robot proposed in this paper consists of a 6-wheel mobile robot. Its design includes a single bogie where the front and middle wheels adhere, a rear wheel connected to the chassis, an additional motor connected to the chassis that utilizes position control to stabilize the delivery package during motion. Many researchers examined kinematic and dynamic analysis based on applications wherein robot wheels are controlled by torque or angular velocity [22-24]. For robots controlled by the angular velocity of the wheels, the studies focus on the forward kinematics and inverse kinematics based on the desired velocity of the robot's CM [25, 26]. Moving the robot by adjusting arbitrary wheels velocity does not guarantee the robot can always reach its destination. Effects such as wheel slip or being stuck are very frequent; therefore, the robot loses its autonomy and requires assistance. Then creating a proper robot control to climb up or down steps, cross uneven terrain, slopes, and potholes

becomes a challenge. Therefore, it is necessary to know the terrain information calculated by the contact point between the wheel and the ground. Several methods, such as a low-cost method by using onboard sensors and an extended Kalman filter, neglect the noise produced by the sensors [27, 28]. There is also installing force and torque sensors at each wheel. However, these methods are expensive and mechanically complex [29, 30]. Cameras and lidar sensors are important methods. Although, it is necessary to install one mono-camera or lidar sensor in each wheel, which is converted into a complex hardware implementation [31]; also, the light condition in the environment affects the results. Another method is to estimate the contact angle from the tilt angles of the robot, although its application is limited to stair climbing [32]. After obtaining information on where the wheel is touching the ground, there are some effects or situations that affect the mobility of the robot, such as a slip or stuck of the wheel. Certain approaches involve analysis of the mobile robot based on dynamics and the interaction between the wheel and the ground, requiring estimation of the friction force [33]. The most common method involves calculating the minimum required friction and optimizing the ideal torque values of the wheels to reduce the risk of slip [34]. That is only possible in autonomous robots controlled by torque. For robots controlled by the angular velocity of the wheels, other methods can be implemented using proper control techniques [35]. Based on the discussion above, the contributions of this study are as follows:

- A mathematical model to control velocity on each wheel according to the desired velocity of the robot's CM, avoiding slip between the wheel-ground.
- Method for estimating contact angle in uneven terrain and special cases, when the robots are climbing up one step using onboard sensors such as IMU and encoders.
- Simulation and results of the performance of the robot motion and contact angle estimation while climbing up one step and uneven terrain.

In Sec. 2, we present the design of the proposed robot, and the kinematic analysis is detailed. Furthermore, the forward kinematics are determined using the Jacobian matrices of each wheel in conjunction with the contact angle estimation between the wheel-ground, and inverse kinematics are determined to obtain the angular velocities of each wheel according to the desired velocity of the robot's center of mass. In Sec. 3, the method to estimate the contact angles between the wheel and ground and slip control is presented. In Sec. 4, a description of the simulation of the robot in Gazebo using ROS and C++ and the validation through the experimental results.

2. Robot design and kinematic analysis

2.1 Robot design

The general purpose of the wheeled robot is to perform outdoor tasks such as delivering packages. It is designed to adapt to different terrains, control its velocity, and avoid slipping, es-

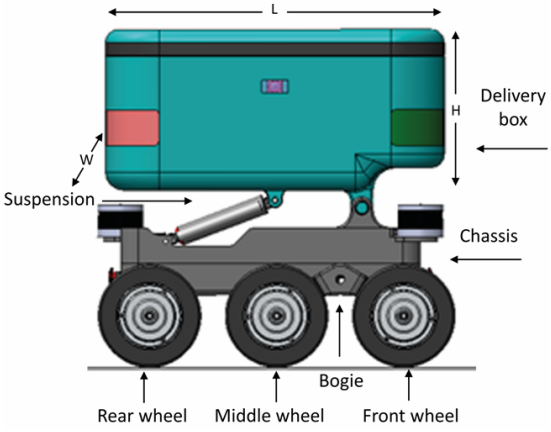

(a) CAD model

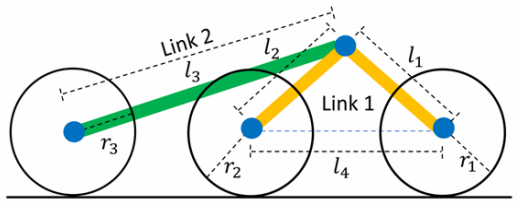

(b) 2D schematic diagram

Fig. 1. Robot design: (a) CAD model of DeepExpress mobile robot by KETI; (b) 2D schematic diagram of the robot mechanism.

sential for optimal performance. The design consists of the payload in the main body, which is always stable irrespective of the robot's pose. As shown in Fig. 1(a) the 3D model, designed by the Korea Electronics Technology Institute (KETI) [36, 37], denotes a 6-wheel robot with a bogie passive revolute joint that connects the front and middle wheels. Furthermore, the rear wheel is attached to the chassis, a suspension system is composed of three cylinders that connect the chassis and the main body to maintain horizontal the delivery package's orientation with respect to the ground while climbing up or down. The prototype presented in the study uses one motor instead of the three cylinders because the robot is on a smaller scale. The analysis of the robot is represented in a 2D schematic diagram as shown in Fig. 1(b), Link 1 is formed by l_1 the distance between the bogie joint and center of the front wheel, and l_2 the distance between the bogie joint and center of the middle wheel. Link 2 is an imaginary formed by l_3, the link between the center of the bogie and the rear wheel. Table 1 shows the dimensions of the small-scale robot used in the experiments and simulations. The IMU was installed in the center of the chassis to obtain the orientation, acceleration, and velocity of the robot, and an encoder was installed in each bogie to determine its position and angular velocity.

2.2 Kinematic constraints

Based on the geometric configuration, the constraints between the links and wheels are shown in Fig. 1(b) and defined in Eq. (1) as follows:

Table 1. Dimension of the small-scale robot (length (L), width (W), height (H), meters (m)).

Parameters	Values (m)
Chassis (L x W x H)	0.22*0.12*0.06
Delivery box (L x W x H)	0.22*0.12*0.05
Wheel radius	0.045
l_1	0.075
l_2	0.075
l_3	0.18
l_4	0.12

(a) To maintain link 1 in a triangular shape and as a rigid body, irrespective of the robot's motion.

(b) To avoid collision between the front and middle wheels, parameter l_4 must exceed the sum of r_1 and r_2.

(c) The bogie connected to the chassis exhibits a turning radius when climbing obstacles up and down. This radius must be less than the length of parameter l_3 to avoid collisions between the middle and rear wheels.

(d) The radius of the wheels r_i where $i = \{1,2,3\}$ must be lower than the parameters l_i where $i = \{1,2,3,4\}$ to avoid collisions between wheels.

$$\begin{cases} l_2 + l_1 \geq l_4; l_2 + l_4 \geq l_1; l_1 + l_4 \geq l_2 \\ l_4 + \geq r_1 + r_2 \\ l_3 - r_3 \geq l_2 + r_2 \\ r_i < l_i. \end{cases} \quad (1)$$

2.3 Forward kinematics

A mobile robot with six wheels individually controlled by each motor is analyzed to determine the relationship between the angular velocity of the wheels and the velocity of the robot's CM considering the contact angle between the wheel-ground. As is known, wheeled robots move on different terrains with different geometric surfaces; it is assumed the terrain is rigid because the robots move in the city. Adjusting arbitrary velocity values on each wheel does not guarantee that the robot can overcome the obstacle due to external effects such as wheel slip. It means kinematic analysis plays a fundamental role in finding the angular velocity of each wheel according to the robot's desired velocity in conjunction with the contact angle between wheel-ground based on the robot's pose, to create a proper control reducing the wheel slip. Links 1 and 2 are considered rigid bodies, which implies that the body does not deform, or the deformation is minimal, and thus it can be neglected. Given the symmetry of the robot, the kinematic model is presented in 2D in Fig. 2(a). In the figure, α_2 denotes the angle between l_2 and x global axis, α_3 denotes the angle between l_3 and x global axis, the coordinate frame $\{F\}$ is the inertial reference frame, $\{O\}$ frame corresponding to the

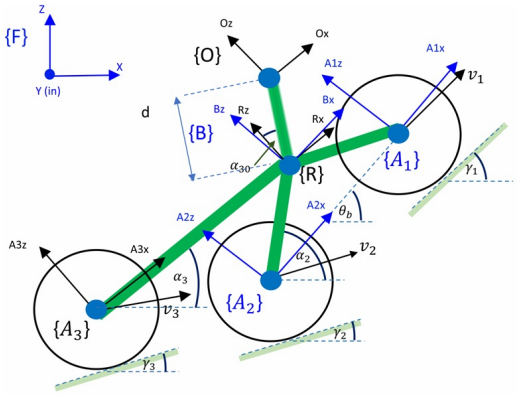

(a) Robot coordinate frames

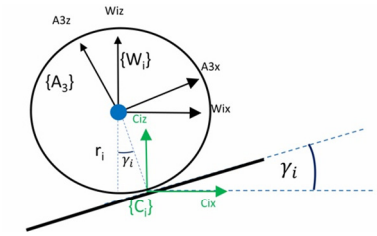

(b) Wheel coordinate frames

Fig. 2. Coordinate frames for KETI robot design.

center of mass, in which the x-axis is parallel to l_3. Furthermore, $\{R\}$ frame corresponds to the bogie joint and rotates with respect to link 2 parallel to frame $\{O\}$, $\{B\}$ frame corresponds to the bogie joint and rotates with respect to link 1, whose x-axis is parallel to l_4. Additionally, $\{A_i\}$, where $i =$ 1, 2, 3, corresponds to the front, middle, and rear wheels, respectively. This frame corresponds to the end of each link whose x-axis is parallel to the longitudinal axis of each link. In Fig. 2(b), the coordinate frames are as follows: $\{A_i\}$, $\{W_i\}$ frame corresponds to the center of each wheel and rotates with respect to each wheel, $\{C_i\}$ frame corresponds to the contact between the wheel and ground. This method uses Sheth-Uicker notation to assign two more coordinates frame about the instantaneous coincident coordinate [25, 38] in frames $\{C_i\}$ and $\{O\}$, that are moving frame thus at every time has a new position and orientation but remain stationary with respect $\{F\}$. The kinematic of the robot are represented using homogeneous transformation matrices, ${}^{A}\boldsymbol{T}_{B} \in \boldsymbol{R}^{4x4}$, which is formed by a rotational matrix $(3x3)$. The matrix which denotes the orientation of the x, y, z axes of coordinate frame $\{B\}$ relative to $\{A\}$. Furthermore, a translation vector $(3x1)$ denotes the displacement of origin $\{B\}$ with respect to origin $\{A\}$ along the x, y, z, axis of $\{A\}$. The coordinate frames ${}^{O}\boldsymbol{T}_{R}, {}^{R}\boldsymbol{T}_{B}, {}^{R}\boldsymbol{T}_{A_3}$ are shown in Fig. 2(a), where the frames $\{O\}$ and $\{R\}$ are aligned, d represents the distance between both origin frames, and α_{30} denotes the initial angle of α_3, i.e., the angle between $\{B\}$ and $\{R\}$ frames when the robot is on a flat surface. In matrix ${}^{R}\boldsymbol{T}_{B}$, where $\{B\}$ is rotated by α_3 along the y-axis, $\{R\}$ and $\{B\}$ have the same origin. In matrix ${}^{R}\boldsymbol{T}_{A_3}$, $\{R\}$ and $\{A_3\}$ frames are parallel. In matrices

${}^{B}\boldsymbol{T}_{A_1}$ and ${}^{B}\mathbf{T}_{A_2}$, $\{A_1\}$ and $\{A_2\}$ frames are parallel with respect to $\{B\}$ frame and only exhibit translation. Fig. 2(b) shows $\{W_i\}$ frames, $i=\{1,2,3\}$, which correspond to front, middle, and rear wheels, respectively. The frame corresponds to the center of each wheel and rotates with respect to the y-axis. Additionally, $\{W_i\}$ and $\{A_i\}$ frames are in the same origin, and thus only rotation exists. Finally, ${}^{W_i}\boldsymbol{T}_{C_i}$ shows the relation between the wheel and contact angle $\{W_i\}$ and $\{C_i\}$ frames respectively. Based on Ref. [25], which presented an analysis of the kinematic equation of wheeled mobile robots with the contact point between the wheel and ground. We obtain the Jacobian matrix that relates the angular velocity of each wheel and desired velocity of the robot's CM Eq. (2) where $\dot{p}$ denotes the desired robot velocity, where V_{o_x} and V_{o_z} denote linear velocities in the x and z axes, respectively, and w_o denotes the angular velocity along the y-axis and $\dot{q}$ denotes the angular velocity of each wheel W_i $i=\{1,2,3\}$, correspond front, middle and rear wheel respectively. Eq. (3).

$$\dot{\boldsymbol{p}}=\boldsymbol{J}_i\dot{\boldsymbol{q}} \tag{2}$$

$$\dot{\boldsymbol{p}}=\begin{bmatrix}V_{o_x}\\V_{o_z}\\w_o\end{bmatrix},\ \dot{\boldsymbol{q}}=\begin{bmatrix}w_1\\w_2\\w_3\end{bmatrix} \tag{3}$$

To obtain each wheel's Jacobian matrix, it is necessary to calculate the displacement between the origins of frames $\{O\}$ and $\{A_i\}$, which correspond to the transformation matrix ${}^{O}T_{A_i}$ Eq. (4), the value of row and column (1, 4) and (3, 4) denote ${}^{O}d_{A_{ix}}$ and ${}^{O}d_{A_{iz}}$, respectively, as follows:

$${}^{O}\boldsymbol{T}_{A_i}={}^{O}\boldsymbol{T}_{R}\cdot{}^{R}\boldsymbol{T}_{P}\cdot{}^{P}\boldsymbol{T}_{A_i} \tag{4}$$

The Jacobian matrices are as follows:

$$\boldsymbol{J}_1=\begin{bmatrix}r_1\left[\cos(\gamma_1)\cos(\alpha_3)+\sin(\gamma_1)\sin(\alpha_3)\right]-{}^{O}d_{A_{1z}}\\r_1\left[\sin(\gamma_1)\cos(\alpha_3)-\cos(\gamma_1)\sin(\alpha_3)\right]-{}^{O}d_{A_{1x}}\\1\end{bmatrix} \tag{5}$$

$$\boldsymbol{J}_2=\begin{bmatrix}r_2\left[\cos(\gamma_2)\cos(\alpha_3)+\sin(\gamma_2)\sin(\alpha_3)\right]-{}^{O}d_{A_{2z}}\\r_2\left[\sin(\gamma_2)\cos(\alpha_3)-\cos(\gamma_2)\sin(\alpha_3)\right]-{}^{O}d_{A_{2x}}\\1\end{bmatrix} \tag{6}$$

$$\boldsymbol{J}_3=\begin{bmatrix}r_3\left[\cos(\gamma_3)\cos(\alpha_3)+\sin(\gamma_3)\sin(\alpha_3)\right]-{}^{O}d_{A_{3z}}\\r_3\left[\sin(\gamma_3)\cos(\alpha_3)-\cos(\gamma_3)\sin(\alpha_3)\right]-{}^{O}d_{A_{3x}}\\1\end{bmatrix} \tag{7}$$

where $\boldsymbol{J}_1$, $\boldsymbol{J}_2$ and $\boldsymbol{J}_3$ denote the Jacobian matrix of the front, middle and rear wheel, respectively.

2.4 Inverse kinematic

Subsequently, the inverse of the Jacobian matrix is derived from Eq. (8) where $\dot{\boldsymbol{q}}$ $(3x1)$ is the angular velocity of each wheel based on the desired velocity of the robot center of mass $\dot{\boldsymbol{p}}$ $(3x1)$, $\boldsymbol{J}^{-1}$ denotes the inverse of Jacobian matrix $(3x3)$, which includes the Jacobian of each wheel Eqs. (5)-(7), thus we can obtain Eq. (8) as follows:

$$\begin{bmatrix}w_1\\w_2\\w_3\end{bmatrix}=\left[\boldsymbol{J}_1\ \boldsymbol{J}_2\ \boldsymbol{J}_3\right]^{-1}\begin{bmatrix}V_{o_x}\\V_{o_z}\\w_o\end{bmatrix} \tag{8}$$

However, it is crucial to check if the inverse is possible for al cases. Therefore, the Jacobian matrix needs to avoid these characteristics: 1) The Jacobian matrix not being a square matrix and 2) the robot being in singularity, which means the robot lost a DOF due to the Jacobian matrix losing its rank, the determinant of Jacobian becomes zero, and the inverse does not exist, which means the robot has lost a DOF. In the proposed model, the robot configuration does not have these problems; therefore, it is possible to use the inverse of the Jacobian. Prior to calculating the Jacobian matrices, it is necessary to obtain the contact angle between the wheel-ground. however, it is difficult to measure contact angles in the real world. Thus, the method used to estimate the contact angles is presented in the next section.

3. Wheel-ground contact angle estimation

Unlike other contact angle estimation methods based on external sensor [29-31] such as force and torque sensors and mono cameras, which require complex installation and powerful data acquisition, our method creates a strategy using onboard sensors to estimate the contact angle between the wheel-ground based on rigid-body kinematic equations. Instead of arbitrarily adjusting the velocity values on each wheel, as if the robot were moving only on a flat surface, we can create a proper robot control according to different geometric terrains, such as steps, slopes, and uneven terrain, guaranteeing that the robot climbs successfully. Otherwise, the robot may fail in its attempt to climb due to the slip in between wheel-ground. Thus, the contact angle is defined as the angle between the gravity force and the vector from the wheel center and wheel-ground contact point. Furthermore, it is the angle between the linear velocity of the wheel and plane tangent to the point of contact γ_i Fig. 2(b). The six wheels include independent actuators, and the following assumptions are made:

1. The ground is rigid.
2. The wheels contact the ground at a single point.
3. There is no-slip between the wheel and ground.

It is reasonable to assume that the terrain is rigid because the environment for delivery robots corresponds to a city. Consequently, the contact between the wheel and ground is around one point as opposed to deformable terrains, such as in space or sand, where the wheels have many contact points. Furthermore, the implementation of the slip control fulfills the

third assumption in Sec. 3.1. Links 1 and 2 are considered as rigid bodies. The distance between the center of the rear wheel and bogie, l_3, is constant and this also holds for l_1, l_2, and l_4. Additionally, θ_b denotes the bogie pitch, and v_1, v_2, and v_3 denote the wheel center velocities and are parallel to the tangent plane at the point of the ground contact. Furthermore, α_2 denotes the angle between l_2 and x global axis, and γ_1, γ_2, and γ_3 denote the contact angles in the front, middle, and rear wheels, respectively, as shown in Fig. 2(a). Eq. (9) indicates that the constraint l_4 does not change because link 1 is a rigid body. Velocities v_1 and v_2 along the direction of l_4 are equal in any motion of the mobile robot. Eq. (10) shows the rigid-body kinematic relation involving the wheel velocities and pitch rate, $\dot{\theta}_b$.

$$v_1 \cos(\gamma_1 - \theta_b) = v_2 \cos(\gamma_2 - \theta_b) \tag{9}$$

$$v_1 \sin(\gamma_1 - \theta_b) - v_2 \sin(\gamma_2 - \theta_b) = l_4 \dot{\theta}_b \tag{10}$$

We combine Eqs. (9) and (10) to obtain the contact angle of the front and middle wheels and is given as follows:

$$\gamma_1 = \theta_b + \sin^{-1}\left(\frac{l_4^2\dot{\theta}_b^2 + v_1^2 - v_2^2}{2l_4\dot{\theta}_b v_1}\right) \tag{11}$$

$$\gamma_2 = \theta_b + \sin^{-1}\left(\frac{v_1^2 - l_4^2\dot{\theta}_b^2 - v_2^2}{2l_4\dot{\theta}_b v_2}\right) \tag{12}$$

To calculate γ_3, the linear velocity of the bogie rotates with respect to the instantaneous center of rotation. In addition, r_{c_1}, r_{b_1}, and r_{c_2} are perpendicular to the velocity vectors v_1, v_b, and v_2, respectively. The linear velocity of the bogie is given as follows:

$$V_b = r_{b1}\dot{\theta}_b \tag{13}$$

$\dot{\theta}_b$ denotes the angular velocity of the bogie that is obtained with the encoder. The design parameter of l_2 is known, and it is necessary to calculate r_{c_2} in Eq. (14) to obtain r_{b_1} in Eq. (15).

$$r_{c_2} = l_4 \frac{\sin 90° - \gamma_1 + \theta_b}{\sin \gamma_1 - \gamma_2} \tag{14}$$

$$r_{b1} = \sqrt{r_{c_2}^2 + l_2^2 - 2r_{c_2}l_2\cos(90° + \gamma_2 - \theta_b - \alpha_{30})} \tag{15}$$

Links 1 and 2 are connected in the bogie joint, and the constraint, where the distance between the center of the rear wheel and bogie joint does not change, is provided in Eq. (16). Furthermore, γ_3 denotes the contact angle of the rear wheel and is given as follows:

$$\gamma_3 = \cos^{-1}\left(\frac{v_b}{v_3}\cos(\theta_b - \alpha_2)\right) + \alpha_2 \tag{16}$$

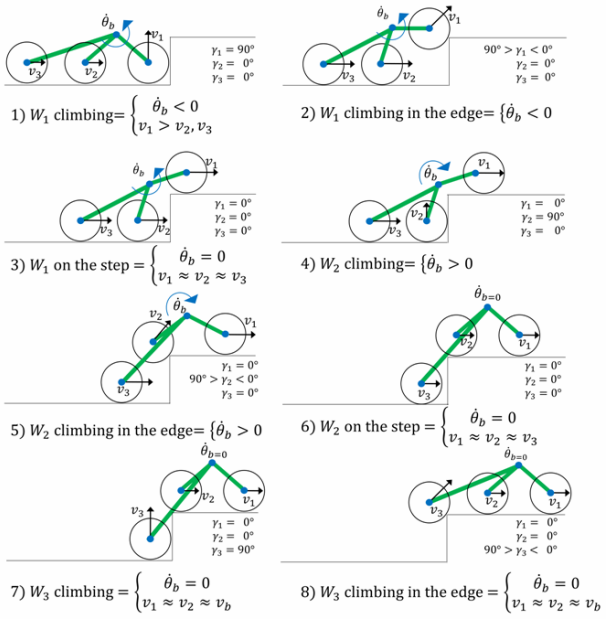

Fig. 3. Delivery robot during climbing up one step and contact angle in each phase.

Eqs. (11) and (12) estimate the contact angles of the front and middle wheels, and Eqs. (13)-(16) are used to estimate the rear wheel. Fig. 3 shows the robot climbing up one step and the contact angle in each phase. Before using these equations, we can simulate and calculate the contact angle by the position of each wheel and the step to have the real contact angle, thus allowing us to observe and analyze the performance of the control with real information about the geometry of the terrain. Then we can compare the performance with the contact angle estimation with the proposed method; the results of simulation and experiment are shown in Sec. 4. When the first wheel started to climb, the angular velocity of the bogie $\dot{\theta}_b$ is counterclockwise and negative as shown in phases 1, 2, and 3; The contact angles of the middle and rear wheels, γ_2 and γ_3, correspond to 0° and the front wheel is 90° during phase 1, then in phase 2 γ_1 reduce from 90° to 1° and 0 ° in phase 3. In phases 4 and 5, when the middle wheel is climbing up, it means γ_2 is equal to 90° phase 4 and reduce until 0° in phase 5 and 6, the angular velocity of the bogie $\dot{\theta}_b$ is positive in the clockwise direction, also the contact angles of the front and rear wheels on flat surfaces γ_1 and γ_3 correspond to 0°. Finally, the angular velocity of the bogie $\dot{\theta}_b$ corresponds to zero when the rear wheel is climbing up in phases 6, 7, and 8. The velocities of the front and middle wheels are similar in the flat surface $v_1 = v_2$, and γ_1 and γ_2 then correspond to zero. The special cases in Eqs. (11), (12) and (16) cannot be used under the following conditions: the first case, if the denominator is zero, we cannot compute the contact angle, this physical mean when the robot is stationary, v_1, v_2, v_3, and $\dot{\theta}_b$ are zero. Eqs. (11)-(16) do not include a solution, and an infinite possible contact angle solution exists at each wheel. The second case occurs when the angular velocity of the bogie is zero or con-

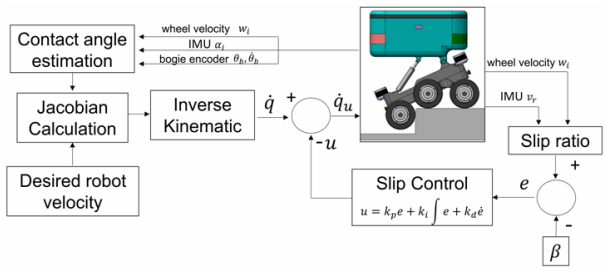

Fig. 4. Overall control schematic of the mobile robot.

stant, and $v_1 \approx v_2$ or $v_1 \approx v_2 \approx v_3$. It occurs when each wheel touches a flat terrain. θ_b is zero in phases 1 and 8 and constant in phases 3 and 6. This implies that γ_1 and γ_2 are zero, or in slope, the contact angles are θ_b. The third case occurs if the arcsine or arccosine in Eqs. (11), (12) and (16) go out of the function range between [-1 to 1], which means that the equation does not present a solution. Thus, it is recommended the value of the contact angle corresponds to the previous value assuming the terrain varies slowly with respect of each wheel.

3.1 Slip control

In Sec. 2, we have calculated the angular velocity of each wheel according to the desired velocity of the robot's center of mass and the geometry terrain from the contact angle information Sec. 3. However, when the robot attempts to climb steps, the slip between the wheel-ground prevents the robot from climbing. This is where the slip control kicks in and actively reduces each wheel's angular velocity to achieve successful climbing without slipping. Fig. 4 shows the schematic of the robot control. The linear velocity of each wheel, orientation of the chassis determined by IMU, and position and velocity of the bogie are used to calculate the contact angle between the wheel-ground in conjunction with the desired robot's body velocity. The Jacobian and its inverse are calculated to compute the velocity of each wheel $\dot{\mathbf{q}}$. Then the slip control signal (u) acts when the slip ratio (S) exceeds threshold (β) and reduces each wheel's angular velocity $\dot{\mathbf{q}}_\mathbf{u}$ to avoid the slip. The slip ratio S Eq. (17) is computed with the robot body velocity instead of the linear velocity of the wheel in Ref. [19], which only can obtain the precise value in simulation. Then S is given as follows:

$$S = \frac{r\dot{\theta}_w - v}{r\dot{\theta}_w} \tag{17}$$

where r denotes the radius of the wheel, $\dot{\theta}_w$ denotes the angular velocity of the wheel, and v denotes the linear velocity of the CM of the robot. Theoretically speaking, S = 0 means no-slip. In our application, we use a threshold β to judge the wheel slip condition. β can be determined from S by observation when slipping begins in real experiments Eq. (18).

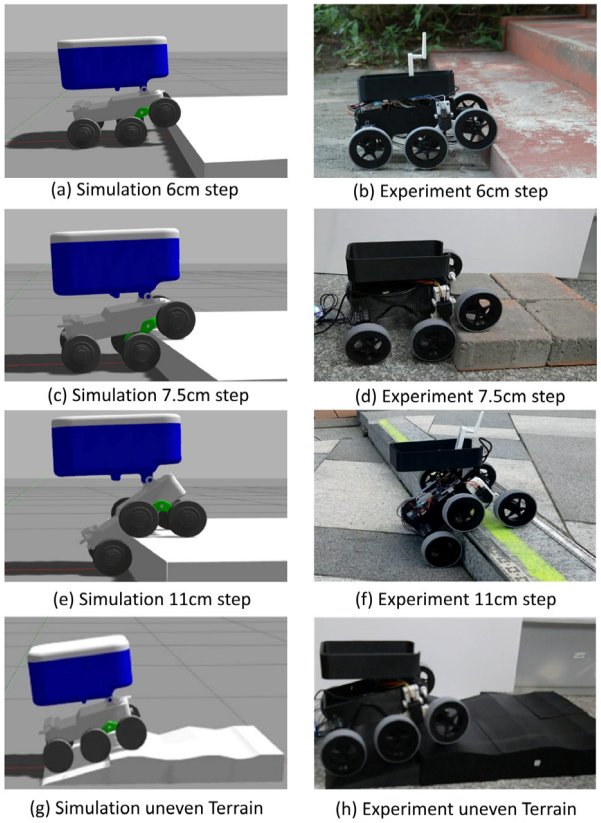

Fig. 5. Simulation and experiment while climbing one step: (a)-(b) 6 cm height step; (c)-(d) 7.5 cm height step; (e)-(f) 11 cm height step; (g)-(h) uneven terrain with a slope.

$$\begin{cases} -\beta < S < 0; & \text{Deceleration} \\ S = 0; & \text{No-Slip} \\ 0 < S < \beta; & \text{Acceleration} \\ |S| > \beta; & \text{Slip} \end{cases} \tag{18}$$

The linear velocity of the robot's CM can be estimated by integrating the acceleration obtained from the IMU or using a tracking camera such as Intel RealSense t265. The radius of the wheel is a known parameter, and the angular velocity of the wheels can be obtained from the actuators. Based on the slip ratio, we use a PID control to obtain the control law. If the slip ratio S exceeds β, the PID controller immediately adjusts the velocity to avoid the slippage between the wheel and the ground.

4. Simulation and experiment

The small-scale mobile robot includes six motors, which control the velocity of the wheels (with a radius of 0.045 m), a motor in the chassis to maintain the stability of the delivery package, optical encoders installed in each bogie, and an IMU sensor in the center of the chassis. The mobile robot moves through the following geometry terrains as shown in Fig. 5(a) and (b) 0.06 m high step, (c) and (d) 0.075 m high step, (e) and (f) 0.11 m high step and (g) and (h) uneven terrain with a slope.

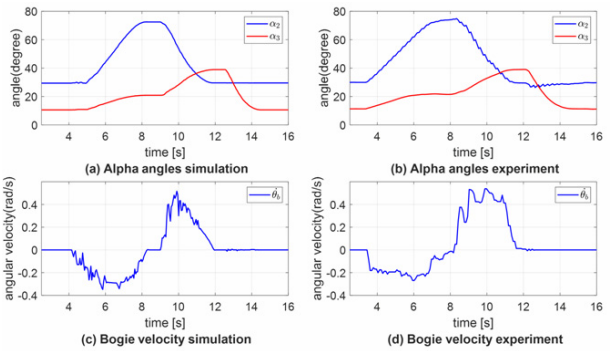

Fig. 6. Simulation during robot climbing up 7.5 cm high step: (a) α_2 and α_3 angles; (c) angular velocity of the bogie. Results (b) and (d) during the experiments.

The results of the climbing robot can be seen in the video link attached below (https://youtu.be/wnI1EbdJMZE). The uneven terrain is different for the wheels on the left and right sides of the robot. The two environments are simulated in Gazebo using ROS. A frequency of 50 Hz was used during simulations and experiments. The IMU in the chassis α_i gets α_3 the angle between l_3 and x global axis. Given by the sum of α_{30} the initial angle of α_3 and the inclination angle of the chassis α_i during robot's motion. The angle also allows the stabilization of the delivery package by the position-controlled motor. Furthermore, α_2 the angle between l_2 and x global axis, is the sum of α_{20} the initial angle of α_2 and the variation of the angle of the bogie obtained by the encoder. Fig. 6(a) shows the angle of α_2 and α_3, and (c) shows the angular velocity of the bogie in the simulation. Figs. 6(b) and (d) show the results of the experiment when the robot climbs up 0.075 height step.

To guarantee the performance of autonomous robots, it is necessary to get information on the terrain and establish an appropriate robot control according to where the contact between the wheel-ground is. The results of contact angle estimation when the robot was climbing up different height steps (6 cm, 7.5 cm, and 11 cm) were shown in Fig. 7. In the simulation, the contact angle was calculated using the position of the step and wheels. In the experiment, results were obtained by Eqs. (11), (12) and (16), as described in Sec. 4. γ_1, γ_2 and γ_3 are the contact angle of the front, middle, and rear wheels respectively. Figs. 8(a), (c) and (e) show the velocity of the robot's CM while climbing one step of 6 cm, 7.5 cm, and 11 cm height, respectively. That can be estimated by integrating the acceleration of the IMU or using tracking sensors, such as the t265 camera. The figure also shows the decreasing velocity of the robot's center of mass when each wheel begins climbing up. Figs. 8(b), (d) and (f) show the linear velocity of each wheel on the left side of the robot climbing the step of 6 cm, 7.5 cm, and 11 cm height, respectively.

The slip ratio was calculated from Eq. (17) to create a proper control of the robot as shown in Fig. 9, slip ratio S and slip control u of the front and middle wheel during climbing up the steps (6 cm, 7.5 cm, and 11 cm). It is verified from the figures

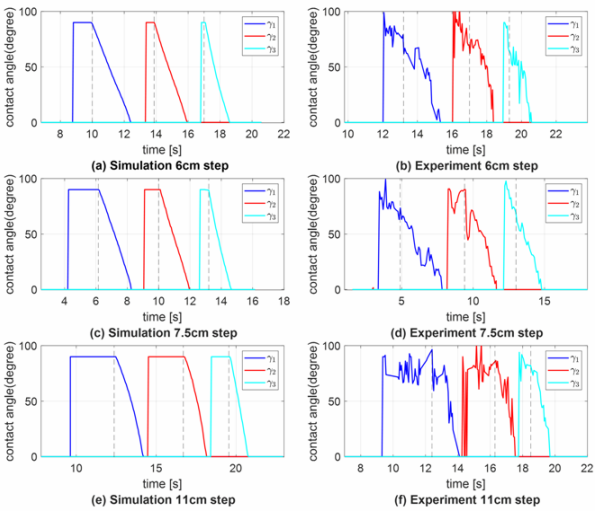

Fig. 7. Simulation of contact angle estimation through climbing up one step of (a) 6 cm; (c) 7.5 cm; (e) 11 cm of height. Results (b), (d) and (f) during experiment.

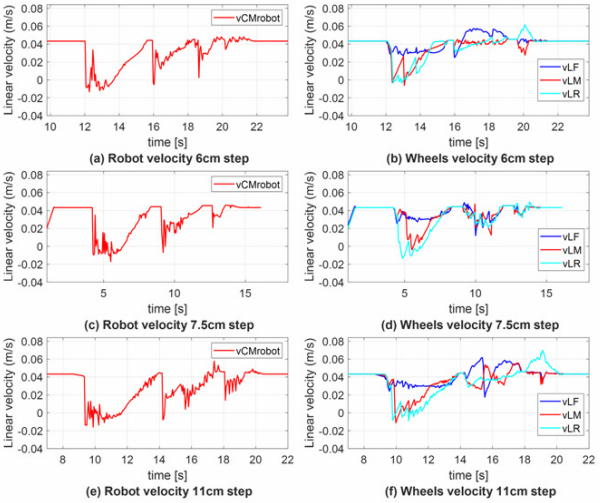

Fig. 8. Robot velocity of the center of mass and linear velocity of each wheel when the robot climbed up one step of 6 cm, 7.5 cm, and 11 cm height (blue, red, and cyan colors represent the front, middle, and rear wheels respectively).

that when the slip ratio exceeds the boundary value of beta (0.6), the controller actively reduces each wheel's angular velocity to avoid the slip, thus achieves successful climbing without slipping. Due to the importance of the geometry terrain to control the robot properly, the contact angle method was also validated on uneven terrain. It was designed and printed in 3d as shown in the Fig. 10(a) left side and (b) ride sight of the uneven terrain, the contact angle estimation on uneven terrain (c) the left side and (d) right side.

The results on the two sides differ because of the geometry differences in the terrain. The robot begins to climb a slope at 16°, which is observed in the time range from 2 to 5 s. The

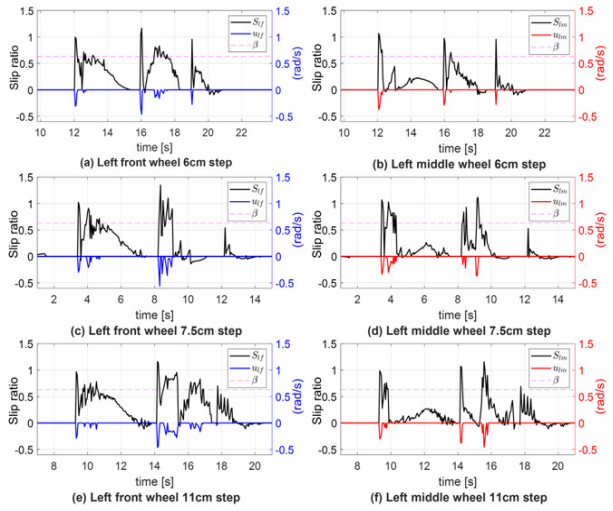

Fig. 9. Slip ratio S and slip control u results of left front wheel (lf) and left middle wheel (lm) when the robot climbed up the steps of 6 cm, 7.5 cm and 11 cm height: (a) 6 cm, lf; (b) 6 cm, lm; (c) 7.5 cm, lf; (d) 7.5 cm, lm; (e) 11 cm, lf; (f) 11 cm, lm.

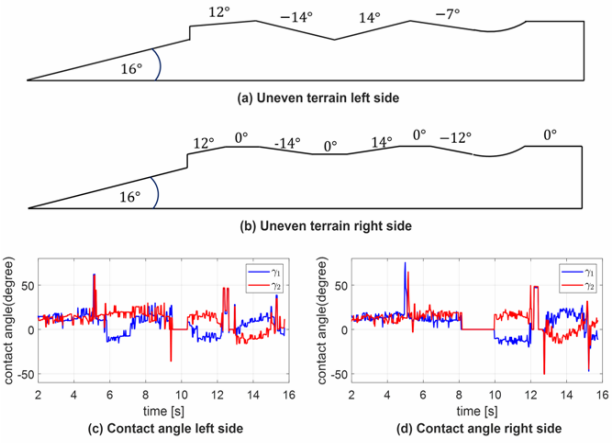

Fig. 10. Wheel-ground contact angle estimation: (a) and (b) uneven terrain design; (c) contact angle of the front γ_1, and middle wheel γ_2 in the left side; (d) contact angle of the front γ_1, and middle wheel γ_2 in the right side.

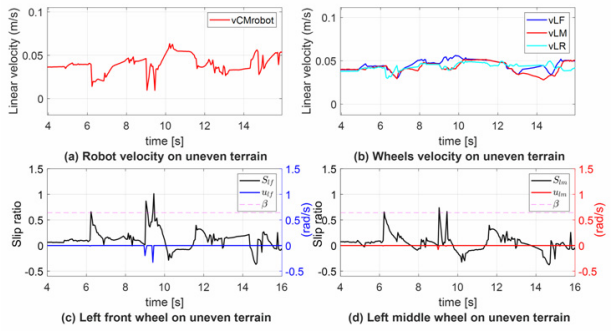

Fig. 11. Robot velocity of the center of mass, the linear velocity of each wheel, slip ratio and slip control on the robot's left side when climbing up on uneven terrain.

uneven terrain presents slopes between 14° and -14°. When the front wheel goes up, the middle wheel goes down, the contact angle of the front wheel is positive, and the middle wheel is negative and vice versa based on the uneven terrain. The contact angle corresponds to 0° when the wheels touch a flat surface. Fig. 11 shows (a) the velocity of the robot's center of mass, (b) the linear velocity of each wheel, (c) and (d) the slip ratio and slip control when robot climbing up uneven terrain, as seen in seconds 8 and 10. The front and middle wheels slip, and the controller acts immediately to prevent slippage. Showing its effectiveness on uneven terrain.

5. Conclusions

In the study, the mobile robot successfully climbs and moves over an uneven terrain and avoids slipping. The results of the estimation of the contact angle successfully verify through simulation and experiments. This in turn will provide a good control of different robots that operate in a city. Kinematic analysis of the robot indicates that it is possible to establish the appropriate velocity for each wheel based on the desired velocity of the robot's CM. Additionally, the IMU in the chassis aids in maintaining the stability of the delivery package throughout its motion.

Acknowledgments

This work was supported by the Industry Core Technology Development Project, 20005062, Development of Artificial Intelligence Robot Autonomous Navigation Technology for Agile Movement in Crowded Space, funded by the Ministry of Trade, Industry & Energy (MOTIE, Republic of Korea).

This work was supported by the National Research Foundation of Korea (NRF) grant funded by the Korea government (MSIT) (No. 2020R1A4A1018227).

References

[1] M. B. Alatise and G. P. Hancke, A review on challenges of autonomous mobile robot and sensor fusion methods, *IEEE Access*, 8 (2020) 39830-39846.

[2] F. Rubio, F. Valero and C. Llopis-Albert, A review of mobile robots: concepts, methods, theoretical framework, and applications, *International Journal of Advanced Robotic Systems*, 16 (2) (2019) 1-22.

[3] Pandey, Mobile robot navigation and obstacle avoidance techniques: a review, *International Robotics Automation Journal*, 2 (3) (2017) 96-105.

[4] H. J. Kim and D. Lee, Single 2D lidar based follow-me of mobile robot on hilly terrains, *Journal of Mechanical Science and Technology*, 34 (9) (2020) 3845-3854.

[5] O. Toupet, J. Biesiadecki, A. Rankin, A. Steffy, G. Meirion-Griffith, D. Levine, M. Schadegg and M. Maimone, Terrain-adaptive wheel speed control on the Curiosity Mars rover: Algorithm and flight results, *Journal of Field Robotics*, 37 (5)

(2020) 699-728.
[6] R. A. Lindemann and C. J. Voorhees, Mars exploration rover mobility assembly design, test and performance, *IEEE International Conference on Systems, Man and Cybernetics*, 1 (2005) 450-455.
[7] J. P. Grotzinger, J. Crisp, A. R. Vasavada, R. C. Anderson, C. J. Baker, R. Barry, D. F. Blake, P. Conrad, K. S. Edgett, B. Ferdowski, R. Gellert, J. B. Gilbert, M. Golombek, J. Gómez-Elvira, D. M. Hassler, L. Jandura, M. Litvak, P. Mahaffy, J. Maki, M. Meyer, M. C. Malin, I. Mitrofanov, J. J. Simmonds, D. Vaniman, R. V. Welch and R. C. Wiens, Mars science laboratory mission and science investigation, *Space Science Reviews*, 170 (2012) 5-56.
[8] B. Hichri, J.-c. Fauroux, L. Adouane, I. Doroftei and Y. Mezouar, Design of cooperative mobile robots for co-manipulation and transportation tasks, *Robotics and Computer Integrated Manufacturing,* 57 (2019) 412-421.
[9] E. Tuci, M. H. M. Alkilabi and O. Akanyeti, Cooperative object transport in multi-robot systems a review of the state-of-the-art, *Frontiers in Robotics and AI,* 5 (2018).
[10] H. S. Hong, T. W. Seo, D. Kim, S. Kim and J. Kim, Optimal design of hand-carrying rocker-bogie mechanism for stair climbing, *Journal of Mechanical Science and Technology*, 27 (1) (2013) 125-132.
[11] B. Choi, G. Park and Y. Lee, Practical control of a rescue robot while maneuvering on uneven terrain, *Journal of Mechanical Science and Technology*, 32 (5) (2018) 2021-2028.
[12] A. Jacoff, B. Weiss and E. Messina, Evolution of a performance metric for urban search and rescue robots, *Proceedings of the 2003 Performance Metrics for Intelligent Systems* (2003).
[13] A. G. Goldhoorn, R. Alquézar and A. Sanfeliu, Searching and tracking people with cooperative mobile robots*, Autonomous Robots*, 42 (4) (2018) 739-759.
[14] K. Nagatani, A. Yamasaki, K. Yoshida and T. Adachi, Development and control method of six-wheel robot with rocker structure, *IEEE International Workshop on Safety, Security and Rescue Robotics* (1) (2007) 2-7.
[15] G. Fragapane, R. de Koster, F. Sgarbossa and J. O. Strandhagen, Planning and control of autonomous mobile robots for intralogistics: literature review and research agenda, *European Journal of Operational Research,* 294 (2) (2021) 405-426.
[16] J. Kim and D. Lee, Mobile robot with passively articulated driving tracks for high terrain ability and maneuverability on unstructured rough terrain: design, analysis, and performance evaluation, *Journal of Mechanical Science and Technology*, 32 (11) (2018) 5389-5400.
[17] C. Wang, L. Meng, S. She, I. M. Mitchell, T. Li, F. Tung, W. Wan, M. Q. Meng and C. W. de Silva, Autonomous mobile robot navigation in uneven and unstructured indoor environments, *arXiv* (2017) 109-116.
[18] S. Jung, D. Choi, H. S. Kim and J. Kim, Trajectory generation algorithm for smooth movement of a hybrid-type robot Rocker-Pillar, *Journal of Mechanical Science and Technology*, 30 (11) (2016) 5217-5224.
[19] S. S. Samsani and M. S. Muhammad, Socially compliant robot navigation in crowded environment by human behavior resemblance using deep reinforcement learning, *IEEE Robotics and Automation Letters*, 6 (3) (2021) 5223-5230.
[20] A. K. Thueer and R. Siegwart, Comprehensive locomotion performance evaluation of all-terrain robots, *IEEE International Conference on Intelligent Robots and Systems* (2006) 4260-4265.
[21] D. Choi, J. Oh and J. Kim, Analysis method of climbing stairs with the rocker-bogie mechanism, *Journal of Mechanical Science and Technology*, 27 (9) (2013) 2783-2788.
[22] S. Parakh, P. Wahi and A. Dutta, Velocity kinematics-based control of rocker-bogie type planetary rover, *TENCON 2010-2010 IEEE Region10 Conference* (2010) 939-944.
[23] D. Kim, H. Hong, H. S. Kim and J. Kim, Optimal design and kinetic analysis of a stair-climbing mobile robot with rocker-bogie mechanism, *Mechanism and Machine Theory*, 50 (2012) 90-108.
[24] H. Hacot, Analysis and traction control of a rocker-bogie planetary rover, *Ph.D. dissertation*, Massachusetts Institute of Technology (1998).
[25] P. F. Muir and C. P. Neuman, Kinematic modeling of wheeled mobile robots, *Journal of Robotic Systems*, 4 (2) (1987) 281-340.
[26] H. Hong, D. Kim, J. Kim, J. Oh and H. S. Kim, A locomotive strategy for a stair-climbing mobile platform based on a new contact angle estimation, *2013 IEEE International Conference on Robotics and Automation* (2013) 3819-3824.
[27] K. Iagnemma and S. Dubowsky, Traction control of wheeled robotic vehicles in rough terrain with application to planetary rovers, *International Journal of Robotics Research*, 23 (10-11) (2004) 1029-1040.
[28] H. Cevallos, G. Intriago and D. Plaza, Performance of the estimators weighted least square, extended kalman filter, and the particle filter in the dynamic estimation of state variables of electrical power systems, *IEEE International Conference on Automation: Towards an Industry 4.0*, 1 (3) (2019) 1-6.
[29] S. Sreenivasan and B. Wilcox, Stability and traction control of an actively actuated micro-rover, *Journal of Robotic Systems*, 11 (6) (1994) 487-502.
[30] S. Ebrahimi and A. Mardani, A new contact angle detection method for dynamics estimation of a UGV subject to slipping in Rough-Terrain, *Journal of Intelligent and Robotic Systems: Theory and Applications*, 95 (3-4) (2019) 999-1019.
[31] X. L. Xu, H. Fu, B. B. Putra and L. He, Visual contact angle estimation and traction control for mobile robot in rough-terrain, *Journal of Intelligent and Robotic Systems: Theory and Applications*, 74 (3-4) (2014) 985-997.
[32] H. Hong, D. Kim, H. S. Kim, S. Lee and J. Kim, Contact angle estimation and composite locomotive strategy of a stair-climbing mobile platform, *Robotics and Computer-Integrated Manufacturing*, 29 (5) (2013) 367-381.
[33] A. G. Conceicao, M. D. Correia and L. Martinez, Modeling and friction estimation for wheeled omnidirectional mobile robots, *Robotica*, 34 (9) (2016) 2140-2150.
[34] Lamon and R. Siegwart, Wheel torque control in rough terrain-modeling and simulation, *Proceedings IEEE International*

Conference on Robotics and Automation (2005) 867-872.
[35] R. Cajo, T. T. Mac, D. Plaza, C. Copot, R. De Keyser and C. Ionescu, A survey on fractional order control techniques for unmanned aerial and ground vehicles, *IEEE Access*, 7 (2019) 66864-66878.
[36] H.-S. Jeong, T.-K. Kim, D. Y. Kim, B.-J. Jung, H.-J. Song, J. M. Lee, H. Son, S.-H. Kim and J.-H. Hwang, A study on driving stability for climb the kerb of outdoor mobile robot, *The Proceedings of 2020 The Korean Society of Mechanical Engineers Conference* (2020) 1577-1578 [Online] https://www.dbpia.co.kr/journal/articleDetail?nodeId=NODE10527719.
[37] J.-H. Hwang, D. Y. Kim, T.-K. Kim and B.-J. Jung, *Wheel Structure and Moving Body Using the Same to Overcome Obstacles*, Korea Patent No. 10-2019-0167600 (2019) Doi: 10.8080/1020190167600.
[38] D. H. Shin and K. H. Park, Velocity kinematic modeling for wheeled mobile robots, *Proceedings- IEEE international Conference on Robotics and Automation,* 4 (1) (2001) 3516-3522.

Nabih Pico received his B.Sc. degree in Electronic and Telecommunication Engineering from Escuela Superior Politécnica del Litoral (ESPOL), in 2014. From 2014 to 2018, he worked as an Assistant Lecturer in robotics with ESPOL. He joined Sungkyunkwan University, Korea, in 2018 to pursue his Ph.D. in Mechanical Engineering at the Robotics and Intelligent System Engineering Laboratory. His current research interest includes autonomous mobile robot, design, control, and analysis of robot-terrain.

Hong-ryul Jung received his B.SE. degree in Mechanical Engineering and Self-designed Transdisciplinary Studies (Artificial Intelligence) in 2017 from Sungkyunkwan University, South Korea. He is currently a Ph.D. student at the Robotics and Intelligent System Engineering Laboratory of the same university. His main research interest is imitation learning for task and motion planning.

Juan Medrano received his B.Sc. degree in Mechatronics Engineering from Universidad del Valle de Guatemala in 2014 and M.Sc. in the same field from Sungkyunkwan University in 2020, where he currently is a Ph.D. student. His research interests are autonomous robot navigation, computer vision and machine learning.

Meseret Abayebas received the B.Sc. degree in Electrical Engineering from Addis Ababa Institute of Technology, Ethiopia in 2015. Before starting his Ph.D., he worked as an Assistant Lecturer with the Addis Ababa Institute of Technology. He joined Sungkyunkwan University, Korea, in 2016 to pursue his Ph.D. degree with the Robotics and Intelligent System Engineering Laboratory. His current research areas lie in modeling, analysis, and nonlinear control theory with applications to mechatronic systems, including robot manipulators and others. He also works on physical human-robot interaction.

Dong Yeop Kim received his B.S. and M.S. in electrical and electronic engineering from Yonsei University, Seoul, Republic of Korea, in 2008 and 2010, respectively. He is a senior researcher in KETI (Korea Electronics Technology Institute) from 2010, and a Ph.D. candidate in electrical and electronic engineering at Yonsei University. His current research interest includes robot navigation, SLAM, sensor fusion, deep learning, and robotic intelligence.

Jung-Hoon Hwang received his B.S. in electrical and electronic engineering from Yonsei University, Seoul, Republic of Korea, in 1997. He received his M.Sc. and Ph.D. in mechanical engineering from Korea Advanced Institute of Science and Technology (KAIST), in 1999 and 2007, respectively. He is a Principal Researcher in KETI (Korea Electronics Technology Institute) from 2007, and also the Director of the Intelligent Robotics Research Center of KETI. His current research interests include robotic manipulation, robot navigation, haptic, human robot interface, deep learning, and robot intelligence.

Hyungpil Moon received his B.S. and M.S. in mechanical engineering from the Pohang University of Science and Technology, Pohang, South Korea, in 1996 and 1998, respectively. He received his Ph.D. in mechanical engineering from the University of Michigan, Ann Arbor, MI, USA, in 2005. From 2006 to 2007, he was a postdoctoral researcher at the Robotics Institute, Carnegie Mellon University. In 2008, he joined the Faculty of the School of Mechanical Engineering, Sungkyunkwan University, Suwon, South Korea, where he is currently a professor. His current research interests include robotic manipulation, SLAM, and polymer-based sensors and actuators.